ACADEMIC PRESS

Available online at www.sciencedirect.com

SCIENCE DIRECT®

Journal of Colloid and Interface Science 261 (2003) 74–81

JOURNAL OF Colloid and Interface Science

www.elsevier.com/locate/jcis

Latex particle size distribution by dynamic light scattering: novel data processing for multiangle measurements

Jorge R. Vega, Luis M. Gugliotta, Verónica D.G. Gonzalez, and Gregorio R. Meira *

INTEC (Univ. Nacional del Litoral–CONICET), Güemes 3450, (3000) Santa Fe, Argentina

Received 13 September 2002; accepted 2 January 2003

Abstract

Multiangle dynamic light scattering (DLS) provides a better estimate of particle size distributions (PSD) than single-angle DLS. However, multiangle data treatment requires appropriate weighting of each autocorrelation measurement prior to calculation of the PSD. The weighting coefficients may be directly obtained from (i) the autocorrelation baselines or (ii) independent measurement of the average light intensity by elastic light scattering. However, the propagation of errors associated with such procedures may intolerably corrupt the PSD estimate. In this work, an alternative recursive least-squares calculation is proposed that estimates the weighting coefficients on the basis of the complete autocorrelation measurement. The method was validated through a numerical example that simulates the analysis of a polystyrene latex with a bimodal PSD and with "measurements" taken at 10 detection angles. The ill-conditioned nature of the problem determines that the "true" PSD cannot be recovered, even in the absence of errors. A sensitivity analysis was carried out to determine the effect of errors in the weighting coefficients on the PSD recoveries.

Keywords: DLS; Multiangle; PSD; Polymer latex; Inverse problem

1. Introduction

The particle size distribution (PSD) of a polymer latex is an important morphological characteristic that determines the processability and end properties of the material when used as an adhesive, a coating, an ink, or a paint [1]. Most industrial latices are obtained via emulsion polymerizations.

Dynamic light scattering (DLS) is a widely applied technique for estimating the PSD of a polymer latex with particles in the submicrometer range. The instrument basically consists of monochromatic laser light falling onto a dilute latex sample, with a photometer placed at a fixed angle with respect to the incident light to collect the light scattered over a small solid angle. Brownian motion induces temporal fluctuations in the scattered light, and a dedicated digital correlator calculates the autocorrelation function. This raw measurement must be appropriately processed to obtain the PSD or the distribution of diffusion coefficients. Details of the technique are given in [2,3].

At a given scattering angle θ_r, the DLS measurement consists of the (second order) autocorrelation of the light intensity fluctuations. This function is defined by

$$G^{(2)}_{\theta_r}(\tau_j) = \lim_{N_s\to\infty} \frac{1}{N_s} \sum_{k=1}^{N_s} \xi_{\theta_r}(\tau_k)\xi_{\theta_r}(\tau_{k+j}),$$

where ξ_{θ_r} is the scattered light intensity; τ_j is the discrete time delay; and N_s ($> 10^6$) is the total number of light intensity samples. The Siegert equation [2] relates $G^{(2)}_{\theta_r}(\tau_j)$ to the modulus of the (first-order and normalized) autocorrelation function of the electric field, $g^{(1)}_{\theta_r}(\tau_j)$,

$$G^{(2)}_{\theta_r}(\tau_j) = G^{(2)}_{\infty,\theta_r}\left\{1+\beta\left|g^{(1)}_{\theta_r}(\tau_j)\right|^2\right\} \quad (\theta_r = \theta_1, \theta_2, \ldots, \theta_R,\ j = 1, \ldots, M_r), \tag{1}$$

where $G^{(2)}_{\infty,\theta_r}$ is the autocorrelation baseline; β (< 1) is an "instrumental" constant; and M_r is the total number of correlator channels or points of the autocorrelation function measured at θ_r. The average intensity of the scattered light $\langle I_{\theta_r}\rangle$, is related to $G^{(2)}_{\infty,\theta_r}$ through

$$\langle I_{\theta_r}\rangle = \sqrt{G^{(2)}_{\infty,\theta_r}}.$$

* Corresponding author.
E-mail address: gmeira@intec.unl.edu.ar (G.R. Meira).

0021-9797/03/$ – see front matter
doi:10.1016/S0021-9797(03)00040-7

The intensity-based PSD or particle light intensity distribution (PLID) $h_{\theta_r}(D_i)$ $(i = 1, 2, \ldots, N)$ represents the fraction of light intensity scattered at θ_r by particles in the range $[D_i, D_{i+1}]$. Thus, the PLID is by definition normalized; i.e., $\sum_{i=1}^{N} h_{\theta_r}(D_i) = 1$. The PLID is related to $g_{\theta_r}^{(1)}(\tau_j)$ through [4]

$$g_{\theta_r}^{(1)}(\tau_j) = \sum_{i=1}^{N} e^{-\Gamma_0(\theta_r)\tau_j/D_i} h_{\theta_r}(D_i) \quad (\theta_r = \theta_1, \theta_2, \ldots, \theta_R,\ j = 1, \ldots, M_r), \tag{2}$$

with

$$\Gamma_0(\theta_r) = \frac{16}{3}\pi \left(\frac{n_m(\lambda)}{\lambda}\right)^2 \frac{kT}{\eta} \sin^2(\theta_r/2) \quad (\theta_r = \theta_1, \theta_2, \ldots, \theta_R), \tag{3}$$

where λ (nm) is the in vacuo wavelength of the incident laser light; $n_m(\lambda)$ is the real refractive index of the nonabsorbing medium; k $(= 0.0138\ \mathrm{g\,nm^2/s^2\,K})$ is the Boltzmann constant; T (K) is the absolute temperature; and η (g/nm s) is the medium viscosity.

The aim is to find the discrete PSD $f(D_i)$ $(i = 1, 2, \ldots, N)$; where f is the number particle concentration in the range $[D_i, D_{i+1}]$ and N is the (chosen) total number of PSD points that are evenly spaced in the range $[D_{\min}, D_{\max}]$. Each PLID is related to the number PSD, as follows,

$$h_{\theta_r}(D_i) = k_{\theta_r} C_{I,\theta_r}(D_i) f(D_i) \quad (\theta_r = \theta_1, \theta_2, \ldots, \theta_R,\ i = 1, \ldots, N), \tag{4}$$

where k_{θ_r} is a constant (for a given θ_r) that ensures the normalization of $h_{\theta_r}(D_i)$; and the function $C_{I,\theta_r}(D_i)$ is calculated through the Mie theory [5]. $C_{I,\theta_r}(D_i)$ represents the fraction of light intensity scattered at θ_r by a particle of diameter D_i, for fixed values of the light polarization, the laser wavelength, and the refractive indexes of the particles and the medium [5,6]. Substituting Eq. (4) into Eq. (2), one obtains

$$g_{\theta_r}^{(1)}(\tau_j) = k_{\theta_r} \sum_{i=1}^{N} e^{-\Gamma_0(\theta_r)\tau_j/D_i} C_{I,\theta_r}(D_i) f(D_i) \quad (\theta_r = \theta_1, \theta_2, \ldots, \theta_R,\ j = 1, \ldots, M_r). \tag{5}$$

Since $\sum_{i=1}^{N} h_{\theta_r}(D_i) = 1$, Eq. (4) provides

$$k_{\theta_r} = \frac{1}{\sum_{i=1}^{N} C_{I,\theta_r}(D_i) f(D_i)} \quad (\theta_r = \theta_1, \theta_2, \ldots, \theta_R), \tag{6}$$

where the denominator of Eq. (6) is proportional (but not equal) to the light intensity scattered at θ_r. Thus, the k_{θ_r} weighting coefficients are proportional to both $\langle I_{\theta_r}\rangle^{-1}$ and $(\sqrt{G_{\infty,\theta_r}^{(2)}})^{-1}$.

In a real measurement, the PSD is unknown, and therefore Eq. (6) cannot be used to estimate the (absolute) k_{θ_r} coefficients. Also, it may be necessary to modify the concentration of the latex emulsion along the different measurement angles to avoid multiple scattering. Thus, it is convenient to define the dimensionless weighting ratio $k_{\theta_r}^*$ relative to a fixed reference angle θ_1,

$$k_{\theta_r}^* = \frac{k_{\theta_r}}{k_{\theta_1}} = \left(\frac{N_{p,\theta_r}}{N_{p,\theta_1}}\right)\left[\frac{G_{\infty,\theta_1}^{(2)}}{G_{\infty,\theta_r}^{(2)}}\right]^{1/2} = \left(\frac{N_{p,\theta_r}}{N_{p,\theta_1}}\right)\frac{\langle I_{\theta_1}\rangle}{\langle I_{\theta_r}\rangle} \quad (\theta_r = \theta_1, \theta_2, \ldots, \theta_R), \tag{7}$$

where $N_{p,\theta_r}/N_{p,\theta_1}$ is the ratio between the number particle concentration at θ_r and the number particle concentration at θ_1. If the sample concentration remains unaltered along the measurement angles, then $N_{p,\theta_r}/N_{p,\theta_1} = 1$.

The last two equalities of Eq. (7) suggest two simple ways of determining the $k_{\theta_r}^*$ ratios: (i) from the autocorrelation baselines, $G_{\infty,\theta_r}^{(2)}$; or (ii) from independent elastic light-scattering measurements of the average intensities $\langle I_{\theta_r}\rangle$. In both cases, the particle concentration ratios must be known a priori. An added practical difficulty is that some commercial DLS software does not strictly provide $G_{\infty,\theta_r}^{(2)}$, but rather values that are only proportional to the real estimates.

From the PSD, several (measurement-independent) average diameters $\overline{D}_{a,b}$ are defined as follows:

$$\overline{D}_{a,b} = \left[\frac{\sum_{i=1}^{N} f(D_i) D_i^a}{\sum_{i=1}^{N} f(D_i) D_i^b}\right]^{1/(a-b)} \quad (a, b = 1, 2, 3, \ldots,\ a > b). \tag{8}$$

Also, an intensity-based average diameter $\overline{D}_{\mathrm{DLS}}$ is defined by

$$\overline{D}_{\mathrm{DLS}}(\theta_r) = \frac{\sum_{i=1}^{N} h_{\theta_r}(D_i)}{\sum_{i=1}^{N} \frac{h_{\theta_r}(D_i)}{D_i}} = \left[\sum_{i=1}^{N} \frac{h_{\theta_r}(D_i)}{D_i}\right]^{-1} = \frac{\sum_{i=1}^{N} f(D_i) C_{I,\theta_r}(D_i)}{\sum_{i=1}^{N} \frac{f(D_i) C_{I,\theta_r}(D_i)}{D_i}}. \tag{9}$$

Note that $\overline{D}_{\mathrm{DLS}}$ is a function of the measurement angle, and it cannot be associated with any specific $\overline{D}_{a,b}$. However, the following can be proven: (i) for any monodisperse PSD $f(D_0)$, $h_{\theta_r}(D_i)$ is also monodisperse, and $\overline{D}_{\mathrm{DLS}}$ tends to D_0 independently of θ_r; and (ii) for a PSD inside the so-called Rayleigh region (i.e., typically containing particles smaller than 50 nm), $C_{I,\theta_r} \propto D^6$, and therefore $\overline{D}_{\mathrm{DLS}} \cong \overline{D}_{6,5}$. In practice, $\overline{D}_{\mathrm{DLS}}$ is directly calculated from the autocorrelation function through the cummulants method [7]. This method considers $g_{\theta_r}^{(1)}$ as a power series of τ_j, and it does not require the intermediate calculation of $f(D_i)$ or $h_{\theta_r}(D_i)$.

Consider the data treatment of single-angle DLS. Initially, Eq. (1) is applied to obtain $g_{\theta_r}^{(1)}$ from $G_{\theta_r}^{(2)}$. Then, two calculation paths are possible [8]: (1) first estimate $h_{\theta_r}(D_i)$ by inverting Eq. (2), and then calculate $k_{\theta_r} f(D_i)$ through Eq. (4) ("double-step method"); or (preferably) (2) directly estimate $k_{\theta_r} f(D_i)$ by inverting Eq. (5) ("single-step method"). Since k_{θ_r} is only a scaling factor of $f(D_i)$, its estimation is unnecessary in single-angle DLS.

Compared to single-angle estimates, improved PSD estimates can be obtained by multiangle DLS [9,10]. Such improvement is not only a consequence of the larger information content of multiangle measurements, but also the result of better conditioning of the numerical inversion [11]. More specifically, improved estimates are obtained when the analyzed PSDs are broad, with all the particles outside the Rayleigh region. Unfortunately, such advantages are lost when the PSD is narrow or when it falls inside the Rayleigh region [8,12].

The data treatment of multiangle DLS is still a matter of controversy. The aim is to estimate the PSD through Eqs. (1)–(4), by simultaneously processing all of the measurements. To compensate for the differences in the average intensities at each scattering angle, it has been suggested that each autocorrelation measurement be weighted appropriately prior to estimation of the PSD [9,10,12,13]. We shall here implement such weightings with the $k^*_{\theta_r}$ ratios of Eq. (7).

Cummins and Staples [13] used the "double-step" method to estimate a volume (or mass) PSD on the basis of a reference PLID at θ_1, $h_{\theta_1}(D_i)$. This reference PLID was calculated by inversion of Eq. (2), after replacement of $h_{\theta_r}(D_i)$ by $h_{\theta_1}(D_i)[\langle I_i(\theta_r)\rangle/\langle I_i(\theta_1)\rangle]$, where $\langle I_i\rangle$ is the average light intensity scattered by the particles of diameter D_i. The intensity ratio $[\langle I_i(\theta_r)\rangle/\langle I_i(\theta_1)\rangle]$ was evaluated through the Mie theory [5].

Bott [9] estimated the volume PSD in a single operation, without explicitly calculating any weighting coefficient. His approach is equivalent to inverting Eq. (5) with $g^{(1)}_{\theta_r}$ replaced by

$$\sqrt{G^{(2)}_{\theta_r}(\tau_j) - G^{(2)}_{\infty,\theta_r}}$$

and to using weighting coefficients defined by

$$k_{\theta_r} = \left(G^{(2)}_{\infty,\theta_r}\beta\right)^{-1/2}.$$

The problem of this approach is the propagation of errors of $G^{(2)}_{\infty,\theta_r}$ into the PSD.

Bryant and Thomas [12] and Bryant et al. [10] have calculated the weighting coefficients and the PSD in a single operation. Their approach is equivalent to directly inverting Eq. (5) with weighting coefficients defined by $k_{\theta_r}C_{I,\theta_r}(D_i)$. To solve this relatively complicated nonlinear problem, an ad hoc iterative procedure was developed. It was shown that the errors in the average intensities $\langle I_{\theta_r}\rangle$, when determined by elastic light-scattering, were larger than the errors in the autocorrelation baselines $G^{(2)}_{\infty,\theta_r}$.

In this work, a novel data treatment for multiangle DLS is proposed that first estimates the relative weighting ratios on the basis of the complete autocorrelation functions, and then estimates the number PSD by direct inversion of Eq. (5), without calculation of the PLIDs. The proposed procedure is validated with a synthetic numerical example.

2. Theoretical considerations

Consider first the procedure for estimating the PSD with the single-step method. In vectorial notation, Eq. (5) can be rewritten

$$\mathbf{g}^{(1)}_{\theta_r} = k_{\theta_r}\mathbf{F}_{\theta_r}\mathbf{f} \quad (\theta_r = \theta_1, \theta_2, \ldots, \theta_R), \tag{10}$$

where the vectors $\mathbf{g}^{(1)}_{\theta_r}$ $(M_r \times 1)$ and $\mathbf{f}$ $(N \times 1)$ contain the discrete heights of $g^{(1)}_{\theta_r}(\tau_j)$, and $f(D_i)$, respectively, and $\mathbf{F}_{\theta_r}$ is an $(M_r \times N)$ matrix. The elements of $\mathbf{F}_{\theta_r}$ are given by (see Eq. (5))

$$f_{ji}(\theta_r) = e^{-\Gamma_0(\theta_r)\tau_j/D_i}C_{I,\theta_r}(D_i) \quad (j = 1, \ldots, M_r,\ i = 1, \ldots, N). \tag{11}$$

In Eq. (10), let us replace the absolute coefficients k_{θ_r} by $k_{\theta_1}k^*_{\theta_r}$, where θ_1 is a fixed reference angle (Eq. (7)). The resulting equations can be lumped into the single expression

$$\mathbf{g}^{(1)}_R = k_{\theta_1}\mathbf{G}_R\mathbf{f} \tag{12}$$

with

$$\mathbf{g}^{(1)}_R = \begin{bmatrix} \mathbf{g}^{(1)}_{\theta_1} \\ \mathbf{g}^{(1)}_{\theta_2} \\ \vdots \\ \mathbf{g}^{(1)}_{\theta_R} \end{bmatrix}, \qquad \mathbf{G}_R = \begin{bmatrix} k^*_{\theta_1}\mathbf{F}_{\theta_1} \\ k^*_{\theta_2}\mathbf{F}_{\theta_2} \\ \vdots \\ k^*_{\theta_R}\mathbf{F}_{\theta_R} \end{bmatrix}, \tag{13}$$

where $\mathbf{g}^{(1)}_R$ $[(M_1 + \cdots + M_R) \times 1]$ is an augmented vector and $\mathbf{G}_R$ $[(M_1 + \cdots + M_R) \times N]$ is an augmented matrix.

By definition, $k^*_{\theta_1} = 1$. Therefore, Eqs. (12) and (13) must be solved for $k_{\theta_1}\mathbf{f}$, and for the remaining $(R-1)$ unknown $k^*_{\theta_r}$'s. This problem may be solved as in Bryant et al. [10], through a global *nonlinear* inversion. Alternatively, we here propose the following sequential solution: first, estimate the relative weighting coefficients $k^*_{\theta_r}$, and then find $\mathbf{f}$ through the *linear* inversion of (12),

$$k_{\theta_1}\hat{\mathbf{f}} = \mathbf{G}^{[-1]}_R\mathbf{g}^{(1)}_R, \tag{14}$$

where $\hat{\mathbf{f}}$ is an estimate of $\mathbf{f}$ and $\mathbf{G}^{[-1]}_R$ is a regularized pseudo-inverse of $\mathbf{G}_R$.

For the recursive estimation of the $(R-1)$ unknown $k^*_{\theta_r}$'s, let us define the augmented autocorrelation vector $\mathbf{g}^{(1)}_r$,

$$\mathbf{g}^{(1)}_r = \begin{bmatrix} \mathbf{g}^{(1)}_{r-1} \\ \mathbf{g}^{(1)}_{\theta_r} \end{bmatrix} \quad (r = 2, \ldots, R), \tag{15}$$

with $\mathbf{g}^{(1)}_1 = \mathbf{g}^{(1)}_{\theta_1}$. At each recursive step, the "best" $k^*_{\theta_r}$ is found as follows:

(1) calculate the combined matrix

$$\mathbf{G}_r = \begin{bmatrix} \mathbf{G}_{r-1} \\ k^*_{\theta_r}\mathbf{F}_{\theta_r} \end{bmatrix} \tag{16}$$

with $\mathbf{G}_1 = \mathbf{F}_{\theta_1}$;

(2) calculate an estimate of $\mathbf{g}_r^{(1)}$ on the basis of the $(r-1)$ previous measurements with

$$\hat{\mathbf{g}}_r^{(1)} = \mathbf{G}_r\{\mathbf{G}_{r-1}^{[-1]}\mathbf{g}_{r-1}^{(1)}\}, \tag{17}$$

where a weak regularization is recommendable for the inversion indicated in Eq. (17);

(3) calculate the error vector between the augmented autocorrelation vector $\mathbf{g}_r^{(1)}$ and its upgraded estimate $\hat{\mathbf{g}}_r^{(1)}$,

$$\mathbf{e}_r = \mathbf{g}_r^{(1)} - \hat{\mathbf{g}}_r^{(1)}; \tag{18}$$

(4) estimate $k_{\theta_r}^*$ as the value that minimizes the sum of squared errors

$$\min_{k_{\theta_r}^*}\left(\mathbf{e}_r^T\mathbf{e}_r\right). \tag{19}$$

The procedure of Eqs. (15)–(19) is proposed for calculating the $k_{\theta_r}^*$ ratios, but not the PSD. To estimate the PSD, Eq. (14) with $\mathbf{G}_R$ as defined by Eq. (13) is applied. Note that the proposed method does not require the particle concentration ratios to be inputs, since such ratios are implicitly included in the definition of the $k_{\theta_r}^*$ coefficients. The regularization in Eq. (17) must be relatively weak, in the sense that $\{\mathbf{G}_{r-1}^{[-1]}\mathbf{g}_{r-1}^{(1)}\}$ does not provide an acceptable estimate of $\mathbf{f}$. In other words, the regularization of $\mathbf{G}_R$ in Eq. (14) must be stronger than the regularization of $\{\mathbf{G}_{r-1}^{[-1]}\mathbf{g}_{r-1}^{(1)}\}$ in Eq. (17).

3. A simulated example

3.1. Initial measurements

Some initial autocorrelation baseline measurements were carried out to estimate the typical errors of the $k_{\theta_r}^*$ ratios, when estimated through the last equality of Eq. (7). The analyzed latex was a monodisperse polystyrene (PS) from Polyscience, of nominal diameter 306 nm. The dynamic laser light scattering photometer was from Brookhaven Instruments Inc. The instrument was fit with a vertically polarized He–Ne laser at 632.8 nm and a digital correlator (Model BI-2000 AT). The measurements were carried out at 25 °C. Five measurements of the autocorrelation baselines were taken at each of the following detection angles: 30, 50, 70, 90, 110, and 130° (see Table 1a). Each measurement took between 100 and 200 s, and the particle concentration was adjusted as indicated in Table 1a to produce a counting rate of around 200,000 counts/s. Then, a reference angle $\theta_1 = 30°$ was adopted, and the $k_{\theta_r}^*$ ratios were calculated from the $G_{\infty,\theta_r}^{(2)}$ baselines. Table 1b presents the resulting $k_{\theta_r}^*$ ratios and their relative errors with respect to the average values. The relative errors seem to show some dependence with the detection angle. Also, maximum deviations of around ±5% are seen in the $k_{\theta_r}^*$ ratios.

3.2. The simulated measurements

Consider the simulated DLS analysis of a polydisperse PS latex. Some of the sought system parameters are

Table 1

(a) Initial measurements: autocorrelation baselines ($G_{\infty,\theta_r,q}^{(2)} \times 10^{-9}$) for the different combinations of measurement angles, concentration ratios, and measurement number

θ_r	30°	50°	70°	90°	110°	130°
$N_{p,\theta_r}/N_{p,\theta_1}$	1	1.461	2.675	6.427	20.78	85.47
$q=1$	0.4916	0.4170	0.4246	0.4174	0.4737	0.4559
$q=2$	0.4797	0.4970	0.4289	0.4572	0.4707	0.4619
$q=3$	0.5119	0.4755	0.4142	0.4195	0.4750	0.4654
$q=4$	0.5451	0.4723	0.4344	0.4246	0.4718	0.4704
$q=5$	0.5105	0.4310	0.4249	0.4302	0.4721	0.4707
Mean[a]	0.5071[a]	0.4586[a]	0.4254[a]	0.4298[a]	0.4727[a]	0.4649[a]

(b) Initial measurements: calculated weighting ratios (with Eq. (17)) and corresponding relative errors

θ_r	30°		50°		70°		90°		110°		130°	
	$k_{\theta_r,q}^*$	$E_{\theta_r,q}$[c]	$k_{\theta_r,q}^*$	$E_{\theta_r,q}$[c]	$k_{\theta_r,q}^*$	$E_{\theta_r,q}$[c]	$k_{\theta_r,q}^*$	$E_{\theta_r,q}$[c]	$k_{\theta_r,q}^*$	$E_{\theta_r,q}$[c]	$k_{\theta_r,q}^*$	$E_{\theta_r,q}$[c]
$q=1$	1	0%	1.586	3.0%	2.878	−1.5%	6.975	−0.2%	21.17	−1.7%	88.75	−0.6%
$q=2$	1	0%	1.435	−6.7%	2.829	−3.2%	6.583	−5.8%	20.98	2.6%	87.10	−2.5%
$q=3$	1	0%	1.516	−1.5%	2.974	1.8%	7.100	1.6%	21.57	0.2%	89.64	0.4%
$q=4$	1	0%	1.570	2.0%	2.997	2.6%	7.282	4.2%	22.34	3.8%	92.01	3.0%
$q=5$	1	0%	1.590	3.3%	2.932	0.3%	7.001	0.2%	21.61	0.4%	89.01	−0.3%
Mean[b]	1[b]	–	1.539[b]	–	2.922[b]	–	6.988[b]	–	21.53[b]	–	89.30[b]	–

[a] Mean baselines: $\overline{G}_{\infty,\theta_r}^{(2)} = (1/5)\sum_{q=1}^{5} G_{\infty,\theta_r,q}^{(2)}$.

[b] Mean weighting ratios: $\bar{k}_{\theta_r}^* = (1/5)\sum_{q=1}^{5} k_{\theta_r,q}^*$.

[c] Relative error in $k_{\theta_r}^*$: $E_{\theta_r,q} = (k_{\theta_r,q}^*/\bar{k}_{\theta_r}^* - 1) \times 100$.

Table 2
The simulated example: "measurements" and resulting weighting ratios

r	θ_r (°)	$\Delta\tau$ (μs)	$G^{(2)}_{\infty,\theta_r}$ (# × 10^{-9})	Weighting ratios				
				True	With additive error		Estimated	
				$k^*_{\theta_r}$	$k^*_{\theta_r,e}$	E_{θ_r} [a]	$\hat{k}^*_{\theta_r}$	E_{θ_r} [b]
1	30	210	495.68	1	1	0	1	0
2	40	120	258.90	1.3837	1.3740	−0.701	1.3792	−0.325
3	50	75	113.45	2.0903	2.1706	3.842	2.0880	−0.110
4	60	50	42.594	3.4114	3.4242	0.375	3.4075	−0.114
5	70	35	14.450	5.8568	5.9403	1.426	5.8059	−0.869
6	80	24	4.9748	9.9819	9.9892	0.073	9.8242	−1.580
7	90	18	2.0873	15.4103	15.8163	2.635	15.1836	−1.471
8	100	15	1.2242	20.1217	20.6315	2.534	20.0438	−0.387
9	110	13	0.95805	22.7461	22.2369	−2.239	22.6734	−0.320
10	120	13	0.86308	23.9649	23.1817	−3.268	23.7772	−0.783

[a] $E_{\theta_r} = (k^*_{\theta_r,e}/k^*_{\theta_r} - 1) \times 100$.

[b] $E_{\theta_r} = (\hat{k}^*_{\theta_r}/k^*_{\theta_r} - 1) \times 100$.

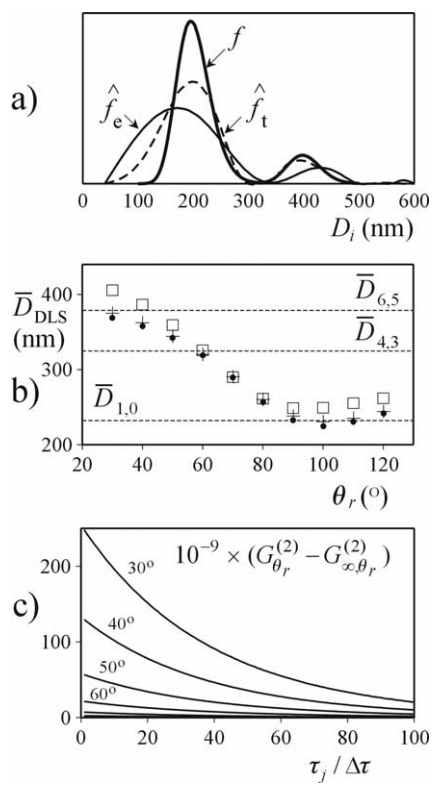

Fig. 1. The simulated example, assuming noise-free autocorrelations. (a) The true number PSD, f, is compared with two estimates. $\hat{f}_t$ (calculated with the "true" $k^*_{\theta_r}$ ratios) and $\hat{f}_e$ (calculated with the erroneous ratios, $k^*_{\theta_r,e}$). (b) The true $\overline{D}_{DLS}$ averages (represented by dots) are compared with the estimated $\overline{D}_{DLS}$ obtained from $\hat{f}_t$ (in crosses) and from $\hat{f}_e$ (in squares). For comparison, other measurement-independent averages $\overline{D}_{a,b}$ are represented. (c) Resulting "measurements" expressed as $(G^{(2)}_{\theta_r}(\tau_j/\Delta\tau) - G^{(2)}_{\infty,\theta_r})$ for different detection angles.

$n_p = 1.5728$ (particle refractive index); $n_m = 1.3316$; $\lambda = 632.8$ nm; $T = 298.15$ K; $\eta = 0.89 \times 10^{-9}$ g/nm s; and $\beta = 0.5$. The synthetic "measurements" were simulated for the detection angles and lag intervals given in the second and third columns of Table 2. The a priori known (discrete and bimodal) PSD is represented by $f(D)$ in Fig. 1a. It consists of 81 equally spaced points in the range [100 nm, 500 nm]. It was obtained by combining two normal-logarithmic distributions,

$$f(D_i) = 0.85\frac{N_p}{D_i\sigma_1\sqrt{2\pi}}\exp\left[-\frac{[\ln(D_i/D_{g,1})]^2}{2\sigma_1^2}\right] + 0.15\frac{N_p}{D_i\sigma_2\sqrt{2\pi}}\exp\left[\frac{[\ln(D_i/D_{g,2})]^2}{2\sigma_2^2}\right], \quad (20)$$

where N_p ($= 10^9$ #/cm^{-3}) is the number particle concentration, $D_{g,1}$ ($= 200$ nm) and $D_{g,2}$ ($= 400$ nm) are the geometric means; and σ_1 ($= 0.150$) and σ_2 ($= 0.075$) are the standard deviations. The distribution averages are represented in Fig. 1b. While $\overline{D}_{1,0}$, $\overline{D}_{4,3}$, and $\overline{D}_{6,5}$ are independent of θ_r, $\overline{D}_{DLS}$ varies from a value that is close to $\overline{D}_{6,5}$ for $\theta_r < 40°$, to a value close to $\overline{D}_{1,0}$ for $\theta_r > 80°$. The reason for this is that while low-angle measurements emphasize the peak with $D_{g,2} = 400$ nm, large-angle measurements emphasize the peak with $D_{g,1} = 200$ nm.

To simplify the analysis, we shall assume that the particle concentration remained unaltered along the simulated experiment, i.e., $N_{p,\theta_r}/N_{p,\theta_1} = 1$. The baselines values were calculated from

$$G^{(2)}_{\infty,\theta_r} = c\left[\sum_{i=1}^{N} C_{I,\theta_r}(D_i)f(D_i)\right]^2 \quad (\theta_r = \theta_1, \theta_2, \ldots, \theta_R), \quad (21)$$

with $c = 10^{-6}$. The resulting baselines are presented in the third column of Table 2. From the baselines and the sought reference angle, the "true" $k^*_{\theta_r}$ ratios were calculated through the second equality of Eq. (7) and are presented in the fourth column of Table 2.

The autocorrelation "measurements" were obtained as follows. First, the noise-free and discrete autocorrelations $G^{(2)}_{\theta_r}(\tau_j)$ with ($j = 1, \ldots, 100$) were calculated through Eqs. (1)–(4), for all the given combinations of θ_r and $\Delta\tau$.

Then, the noisy "measurements" were obtained by adding the following random noise onto the noise-free autocorrelations, $\varepsilon(\tau_j) = 0.001 G^{(2)}_{\infty,\theta_r} \varepsilon_0(\tau_j)$, where ε_0 is a random sequence in the range $[-1, 1]$ with a flat probability distribution [14]. The resulting difference functions $[G^{(2)}_{\theta_r}(\tau_j/\Delta\tau) - G^{(2)}_{\infty,\theta_r}]$ are represented in Fig.1c.

3.3. PSD estimation

Consider recuperating the PSD from the synthetic measurements. First, Eq. (1) was used to calculate $g^{(1)}_{\theta_r}(\tau_j)$ from $G^{(2)}_{\theta_r}(\tau_j)$. Then, a diameter axis was selected for the estimated PSD $\hat{f}(D_j)$ consisting of $N = 29$ equally spaced points in the range $[D_{\min} = 40$ nm, $D_{\max} = 600$ nm$]$. The value of N is a compromise between a highly defined PSD and a well-conditioned inversion. Note that the assumed diameter range of $\hat{f}(D_j)$ is somewhat broader than "real," and that the total number of points is considerably lower than "real." Then, the elements of $\mathbf{F}_{\theta_r}$ were calculated with Eq. (11), and finally the PSD was estimated through Eq. (14).

To solve the pseudo-inverse of $\mathbf{G}_R$ in Eq. (14), two numerical methods were tested: (i) the regularization technique of Twomey [15] with an optimally selected regularization parameter [8], and (ii) the singular value decomposition technique [16]. From all the nonnegative solutions, the "best" PSD estimate $\hat{f}(D_i)$ was selected as that which minimizes the performance index

$$J_f = \left(\frac{\sum_{i=1}^{N} [f(D_i) - \hat{f}(D_i)]^2}{\sum_{i=1}^{N} [f(D_i)]^2} \right)^{0.5}, \tag{22}$$

where $f(D_i)$ is the true PSD. Note that in a real measurement, it would be impossible to calculate J_f. However, this criterion was adopted here to investigate the ultimate limitations of the technique.

Additionally, a performance index was calculated that compares the "true" intensity-based mean diameter $\overline{D}_{\mathrm{DLS}}(\theta_r)$ (obtained by injecting $f(D_i)$ into Eq. (9)) with its estimate $\hat{\overline{D}}_{\mathrm{DLS}}(\theta_r)$ (obtained by injecting $\hat{f}(D_i)$ into Eq. (9)),

$$J_D = \frac{1}{R} \left(\sum_{r=1}^{R} \left[1 - \frac{\hat{\overline{D}}_{\mathrm{DLS}}(\theta_r)}{\overline{D}_{\mathrm{DLS}}(\theta_r)} \right]^2 \right)^{0.5}. \tag{23}$$

Clearly, the PSD that minimizes J_f will not in general minimize J_D.

Consider first recovering the PSD in the totally ideal case of employing the noise-free autocorrelations and the true $k^*_{\theta_r}$ ratios. The resulting solution is $\hat{f}_t(D_i)$ in Fig. 1a, and the performance indexes are shown in the second row of Table 3. Note that large deviations are observed in the recuperated PSD, even in this doubly ideal case. This illustrates the insurmountable limitation of DLS, as a consequence of the highly ill-conditioned nature of the numerical inversion. The condition number of $\mathbf{G}_R$ quantifies the difficulty of the numerical inversion [11]. In our case, this parameter is quite large (7.37×10^{15}), thus indicating a difficult recovery. In contrast, note the almost negligible errors in $\hat{\overline{D}}_{\mathrm{DLS}}(\theta_r)$ (Fig. 1b).

Table 3
The simulated example: performance indices for different combinations of measurements and weighting ratios

Measurements	Weighting ratios	J_f	J_D
Noise-free autocorrelations	$k^*_{\theta_r}$ [a]	0.374	0.0048
	$k^*_{\theta_r,e}$ [b]	0.598	0.0118
Noisy autocorrelations	$k^*_{\theta_r}$ [a]	0.306	0.0149
	$k^*_{\theta_r,e}$ [b]	0.597	0.0118
	$\hat{k}^*_{\theta_r}$ [c]	0.397	0.0279

[a] "True" value.
[b] Value taken from Table 2.
[c] Estimated with the proposed method.

Consider now the propagation of errors of $k^*_{\theta_r}$ into the PSD estimates, when the ideal noise-free measurements are employed, but with $k^*_{\theta_r}$ ratios that are contaminated by an additive error. The noisy ratios are indicated by $k^*_{\theta_r,e}$ and were calculated by adding a random noise of flat probability distribution with an error band of ±4% to the true $k^*_{\theta_r}$. This error band is narrower than the band observed in the initial measurements. The resulting $k^*_{\theta_r,e}$ ratios, together with their errors with respect to the true values, are shown in the sixth and seventh columns of Table 2. The resulting PSD estimate is represented by $\hat{f}_e(D_i)$ in Fig. 1a, and the performance indexes are given in the third row of Table 3. As expected, both J_f and J_D have increased with respect to the totally ideal case.

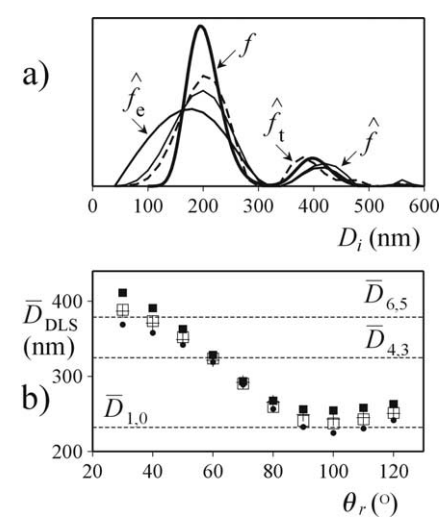

Fig. 2. The simulated example, assuming a zero-mean measurement noise. (a) The true number PSD, f, is compared with the estimates $\hat{f}_t$ (calculated with the "true" $k^*_{\theta_r}$ ratios), $\hat{f}_e$ (calculated with the erroneous $k^*_{\theta_r,e}$ ratios), and $\hat{f}$ (calculated with $\hat{k}^*_{\theta_r}$, as obtained by application of the proposed method). (b) The true $\overline{D}_{\mathrm{DLS}}$ averages (represented by dots) are compared with the estimated $\overline{D}_{\mathrm{DLS}}$ obtained by using $\hat{f}_t$ (in crosses), from $\hat{f}_e$ (in open squares), and from $\hat{f}$ (in full squares). For comparison, other $\overline{D}_{a,b}$ averages are also represented.

Table 4
The simulated example: single- vs multiangle estimations

	30°	60°	90°	120°	Multiangle
Condition number	1.91×10^{19}	1.66×10^{18}	1.15×10^{18}	1.81×10^{18}	7.37×10^{15}
J_f	0.817	0.482	0.543	0.478	0.397
J_D	0.0312	0.0286	0.1805	0.0233	0.0279

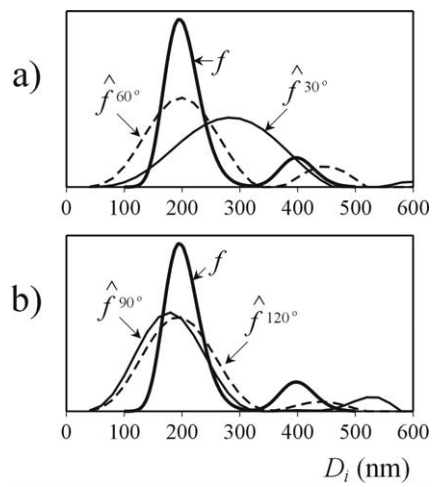

Fig. 3. The simulated example. The original number PSD, f, is compared with several single-angle PSD estimates obtained at (a) 30°, $\hat{f}^{30°}$, and 60°, $\hat{f}^{60°}$, and (b) 90°, $\hat{f}^{90°}$, and 120°, $\hat{f}^{120°}$.

Consider now the more realistic case of using the noisy autocorrelations, but with three different sets of $k^*_{\theta_r}$ values: (i) the "true" coefficients (5th column of Table 2); (ii) the coefficients with errors as given in the previous paragraph (6th column of Table 2); and (iii) the $k^*_{\theta_r}$ estimates obtained by application of the proposed method of Eqs. (15)–(19) (which we shall call $\hat{k}^*_{\theta_r}$). These last estimates, together with their corresponding relative errors, are given in the last two columns of Table 2. The relative errors in $\hat{k}^*_{\theta_r}$ are all lower than 1.6%. Three different PSD estimates were calculated (Fig. 2a). With the "true" ratios, $\hat{f}_t(D_i)$ was obtained. With the $k^*_{\theta_r,e}$ ratios, $\hat{f}_e(D_i)$ was obtained. Finally, $\hat{f}(D_i)$ was obtained from the $\hat{k}^*_{\theta_r}$ ratios. Note that for $\hat{k}^*_{\theta_r}$, the resulting J_f is quite close to the lowest possible value (Table 3).

In Fig. 2b, the "true" $\overline{D}_{\mathrm{DLS}}$ (in dots) are compared with the estimates calculated from $\hat{f}_t(D_i)$, $\hat{f}_e(D_i)$, and $\hat{f}(D_i)$. The J_D values are presented in the last column of Table 3. The inversion methods aimed at minimizing J_f rather than J_D. This explains why the J_D value for $\hat{f}(D_i)$ is larger than that for $\hat{f}_e(D_i)$. Even though not shown in the presented results, $\overline{D}_{\mathrm{DLS}}$ was also estimated by direct application of the cummulants method. The resulting J_D values were lower than those of Table 3.

Finally, the multiangle PSD estimates were compared with the single-angle estimates obtained from the "measurements" at 30, 60, 90, or 120°. The condition numbers of the single-angle inversions are approximately two orders of magnitude higher than those of the multiangle case (Table 4). The resulting PSD estimates are presented in Figs. 3a and 3b, and the performance indexes are given in Table 4. As expected, single-angle measurements produce worse PSD estimates than the multiangle estimate as obtained by application of the proposed procedure. But again, this tendency is not verified for the $\overline{D}_{\mathrm{DLS}}$ mean.

4. Conclusions

Errors in the weighting coefficients may seriously deteriorate PSD estimates of multiangle DLS. A novel method for calculating the weighting ratios has been presented. It involves recursive least-squares and uses all of the measured information. The procedure was tested on a synthetic example, and the numerical results indicate that the weighting ratios are considerably more accurate than those directly obtained from the autocorrelation baselines. An extra advantage of the proposed method is that it does not require independent measurement of the latex concentration, when this variable must be modified along the detection angles.

The proposed procedure aimed at obtaining a number PSD. The technique can be easily extended to determine a volume PSD, with the potential benefit of improving the ill-posedness of the numerical inversion. Also, an iterative (rather than a direct) data treatment could be developed that recalculated the weighting coefficients after a first PSD estimation and finally obtained an improved PSD from the recalculated coefficients. In a future communication, the proposed technique will be verified with real measurements.

Acknowledgments

We are grateful for the financial support received from CONICET, SeCyT, and Universidad Nacional del Litoral (Argentina).

References

[1] R.G. Gilbert, Emulsion Polymerization. A Mechanistic Approach, Academic Press, London, 1995.
[2] R. Pecora, Dynamic Light Scattering. Applications of Photon Correlation Spectroscopy, Plenum, New York, 1985.
[3] B. Chu, Laser Light Scattering, Academic Press, New York, 1991.
[4] S.E. Bott, in: T. Provder (Ed.), Particle Size Distribution. Assessment and Characterization, in: ACS Symp. Ser., Vol. 332, American Chemical Society, Washington, DC, 1987, p. 74.
[5] G. Mie, Ann. Phys. 25 (1908) 337.
[6] C.F. Bohren, D.R. Huffman, Absorption and Scattering of Light by Small Particles, Wiley, New York, 1983.

[7] D.E. Koppel, J. Chem. Phys. 57 (1972) 4814.
[8] L.M. Gugliotta, J.R. Vega, G.R. Meira, J. Colloid Interface Sci. 228 (2000) 14.
[9] S.E. Bott, in: P.J. Lloyd (Ed.), Particle Size Analysis, Wiley, New York, 1988.
[10] G. Bryant, C. Abeynayake, J. Thomas, Langmuir 12 (1996) 6224.
[11] C. De Vos, L. Deriemaeker, R. Finsy, Langmuir 12 (1996) 2630.
[12] G. Bryant, J. Thomas, Langmuir 11 (1995) 2480.
[13] P.G. Cummins, E.J. Staples, Langmuir 3 (1987) 1109.
[14] E. Gulari, Y. Tsunashima, B. Chu, J. Chem. Phys. 70 (1979).
[15] S. Twomey, Franklin Inst. 279 (1965) 95.
[16] J.M. Mendel, Lessons in Estimation Theory for Signal Processing, Communications, and Control, Prentice–Hall, Englewood Cliffs, NJ, 1995.